Study of ablation depth of monocrystalline silicon irradiated by long pulse laser

MING GUO[a,b], YONG-XIANG ZHANG[c,*], YUE-SHU FENG[a,b], SIQI ZHANG[a,b]
[a]Institute for Interdisciplinary Quantum Information Technology, Jilin Engineering Normal University, Changchun 130052, China
[b]Jilin Engineering Laboratory for Quantum Information Technology, Changchun 130052, China
[c]College of Optical and Electronical Information Changchun University of Science and Technology, Changchun 130022, China

In order to explore the erosion morphology and mechanism of monocrystalline silicon irradiated by a laser, an experimental system of millisecond pulsed laser acting on monocrystalline silicon sample was built, and corrosion model was established. The mass conservation of the fluid mechanics, the momentum conservation, and the energy conservation equations were used to describe the entire computational domain. The fluid volume method and the narrow-band level set method were combined to improve the level set control equation. The research shows that after the monocrystalline silicon melts, a molten pool is generated, and a protruding peak structure appears in its center. The laser energy is mainly concentrated at the bottom of the ablation pit. The higher energy density laser acts on the monocrystalline silicon by instantly generating a high temperature. A large recoil pressure is present at the bottom of the pit and causes the molten fluid to flow upward, whereas the viscous shear force and the surface tension make the fluid flow downward. The combination of the opposite flow and the collisions generated such peak structure in the pit. As the laser energy density increases, the presence of the crater shows the ablation morphology change on the sample, the degree of the ablation damage increases, as well as the ablation area. For a fixed laser energy density, as the pulse width increases, the laser power density decreases and the erosion depth and erosion radius decrease. During the re-coagulation process of monocrystalline silicon, ring ripples are formed on its surface. As the number of pulses increases, the laser damage area increases, and the ablation depth increases rapidly with the number of pulses. The experimental and the simulation results are in good agreement. The experimental research carried out verifies the simulation model. This study provides a reference for improving the laser system and broadening its application in scientific research and production.

1. Introduction

Laser technology has been widely used in various industries [1-2]. For this reason, monocrystalline silicon's laser processing has recently become a hot topic. Monocrystalline silicon is a good infrared window material [3-4], and is commonly used as a substrate in optical systems. Monocrystalline silicon may melt under the action of a laser, which may damage its photoelectric function. Previous researches on laser ablation of monocrystalline silicon mainly focused on the study of the action of short pulses and ultrashort pulses, whereas few investigations focused on long pulses lase [5-11]. In 2009, Sha Tao [12] et al studied the vaporization of monocrystalline silicon targets under the action of a laser with a wavelength of 1064 nm and a pulse width of 200 ns. In 2013, C. Fornaroli [13] et al. investigated monocrystalline silicon wafers cut via a picosecond laser. Their results show the relation between the depth and the width of the vaporized monocrystalline silicon grooves, the laser energy and the number of pulses. In 2017, Oskar Armbruster [14] et al. conducted a study on the threshold of the femtosecond laser ablation process of

monocrystalline silicon. In this paper, the simulation model of the monocrystalline silicon's damage caused by a millisecond pulse laser is established. Moreover, the mechanism behind the variation in its ablation depth is explained based on the changes in the laser energy density, pulse width, and number of pulses. The research in this paper may provides a reference for future laser processing of monocrystalline silicon.

2. Numerical simulation

2.1. Model structure

When the laser energy density acting on the monocrystalline silicon is high, the target is eroded. The eroding model structure is shown in Fig. 1. The distribution of the laser energy in the model follows a Gaussian curve, the laser wavelength is 1064 nm, the pulse width is in the 1.0–3.0 ms range (the step measures 0.5 ms), the spot radius is 1.0 mm. The target consists of monocrystalline silicon and has a thickness of 4.0 mm and a radius of 12.7 mm. The air layer has a thickness of 6.0 mm and a width of 12.7 mm.
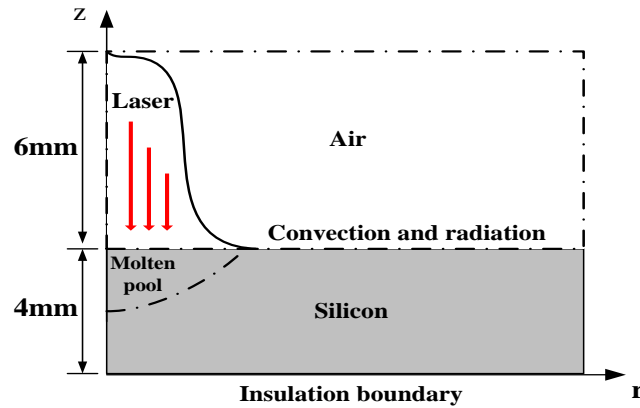
Fig. 1. Geometric model of the monocrystalline ablation induced by laser

Table 1. Physical Parameters of Monocrystalline Silicon [15-18]

Parameter name	Symbol	Dimension	Value or expression
absorption coefficient	α_s	m^{-1}	$1023 \times (T/273)^4$
	α_l	m^{-1}	8.6×10^7
thermal conductivity	k_s	$W \cdot m^{-1} K^{-1}$	$22.23 + 422.52 \times \exp(-T/255.45)$
	k_l	$W \cdot m^{-1} K^{-1}$	62
heat capacity	C_s	$J \cdot kg^{-1} \cdot K^{-1}$	$352.43 + 1.78 \times T - 2.21 \times 10^{-3} T^2 - 1.3 \times 10^{-6} T^3 - 2.83 \times 10^{-10} T^4$
	C_l	$J \cdot kg^{-1} \cdot K^{-1}$	1021.84
density	ρ_s	$kg \cdot m^{-3}$	$2330 - 2.19 \times 10^{-2} T$
	ρ_l	$kg \cdot m^{-3}$	$2540 - 2.19 \times 10^{-2} T - 1.21 \times 10^{-5} T^2$
melting point	T_m	K	1687
Melting latent heat	L_m	J/g	1800
boiling point	T_v	K	3175
boiling latent heat	L_v	J/g	16207
Convective heat transfer coefficient	h	$W \cdot m^{-2} K^{-1}$	20
emissivity	ξ	---	0.17

Note: The subscript "s" means solid and the subscript "I" means liquid.

2.2. Model theory

When a monocrystalline silicon sample is irradiated by a laser with a high energy density, molten spatter is produced when the temperature of the irradiation center point reaches the vaporization temperature of the sample. To describe this phenomenon a two-dimensional axisymmetric laser molten spattering model is established. In the model, the fluid volume method and the narrow-band level set method are combined to improve the level set control equation. The equivalent heat capacity is used to indicate the influence of the latent heat on the phase transition, whereas the liquid target in the molten pool and the ambient air around it are assumed to follow the incompressible Newtonian laminar flow model. Moreover, the Knudsen layer is omitted. The monocrystalline silicon vapor is considered as an ideal gas and it is transparent to the incident laser light. Regardless of the plasma generation, the boiling point of monocrystalline silicon does not change with a variation in the pressure. Three conservation equations were used in this work:

Equation of the Mass Conservation:

$$\nabla \cdot \vec{u} = 0 \qquad (1)$$

In Equation (1), $\vec{u}$ corresponds to the fluid velocity.
Momentum Conservation Equation:

$$\rho \frac{\partial \vec{u}}{\partial t} + \rho(\vec{u} \cdot \nabla)\vec{u} = -\nabla \cdot \left[pI + \mu\left(\nabla \vec{u} + (\nabla \vec{u})^T\right)\right] + \rho \vec{g} + \vec{F}_{vol} \qquad (2)$$

In Equation (2), μ and ρ refer to the kinetic viscosity and the density, respectively.
Energy Conservation Equation:

$$\rho C \frac{\partial T}{\partial t} + \rho C \, \vec{u} \cdot \nabla T = \nabla \cdot (k\nabla T) \qquad (3)$$

In Equation (3), k corresponds to the heat conductivity coefficient of the sample within the calculation area and $\vec{F}_{vol}$ to the volume force.

By taking into account the phase changes that occurs during the interaction between the laser and the monocrystalline silicon target, the enthalpy-vacancy method is introduced to describe the melting and vaporization processes as well as the energy conservation equations while tracking the solid-liquid interface. The thermal energy absorbed by the monocrystalline silicon during the phase change process is affected by the change of enthalpy. In addition, due to the latent heat effect in the phase change process, the specific heat capacity is also affected and begins to change. For this reason, the equivalent specific heat capacity is introduced to solve this problem. Melting occurs when the temperature is within the interval $T_m - \delta T_m \rightarrow T_m + \delta T_m$, whereas the vaporization process takes place in the interval $T_b - \delta T_b \rightarrow T_b + \delta T_b$. The equivalent specific heat capacity can be expressed as:

$$C_{psi,eff} = C + L_m D_m + L_v D_v \qquad (4)$$

Here, T_m is the melting point and T_b the boiling point. L_m corresponds to the melting latent heat,
$D_m = \dfrac{e^{\frac{(T-T_m)^2}{(\delta T_m)^2}}}{\sqrt{\pi \delta T_m}}$, L_v is the gasified latent heat,
$D_v = \dfrac{e^{\frac{(T-T_b)^2}{(\delta T_b)^2}}}{\sqrt{\pi \delta T_b}}$.

The enthalpy-space method was used to track the solid-liquid interface, and the solid-liquid coexistence zone was considered as a fuzzy area of porous material. The unit void ratio corresponds to the liquid fraction. Since the void ratio is zero, the fluid velocity is zero and corresponds to a solid zone. The fuzzy area where the fluid is located can be described by Darcy's law. For example, if the fuzzy area at the interface is solid, the fluid velocity is zero. This phenomenon can be described by defining the momentum deposition:

$$\vec{F}_{vol} = \frac{(1-B)^2}{B^3 + \varsigma} A_{mush}\vec{u} \qquad (5)$$

In equation (5), B refers to the volume fraction of the liquid:

$$B = \begin{cases} 1 & T > (T_m + \delta T) \\ \dfrac{(T - T_m + \delta T)}{2\delta T}, & (T_m - \delta T) \leq T \leq (T_m + \delta T) \\ 0 & T < (T_m - \delta T) \end{cases} \qquad (6)$$

The value ς is small since the denominator cannot be zero, A_{mush} corresponds to the constant of the fuzzy area, and A_{mush} controls the attenuating range of the variable: the larger A_{mush} is, the stronger is the tendency of the velocity to approach zero due to the material solidification.

In this model, not only the interface between the solid and the liquid is taken into account but also the problem of the vapor-liquid interface. Due to the complexity of the physical phenomena at this interface, the Equation at this interface is cumbersome. Hence, the narrow-band level set fluid volume method was used.

The level set control equation is used to describe the interface between a liquid and the vapor:

$$\frac{\partial \phi}{\partial t} + \vec{u} \cdot \nabla \phi + \gamma \left[\left(\nabla \cdot \left(\phi(1-\phi)\frac{\nabla \phi}{|\nabla \phi|}\right)\right) - \varepsilon \nabla \cdot \nabla \phi \right] = 0 \qquad (7)$$

In this Equation, ε and γ are the two parameters of the level set method. ε is related to the thickness of the liquid-gas interface and γ to the flow velocity in the flow field. The modified level set function $\phi(x, y, t)$ can be expressed as: $\phi(x, y, t) = \begin{cases} 0 \\ 0.5 \\ 1 \end{cases}$. Its value is 0 inside the monocrystalline silicon, 0.5 at the liquid-gas interface, and 1 in the ambient gas.

Here, the level set function ϕ is used to define the changes in the parameters of the monocrystalline silicon sample at its interface.

$$\rho = \rho_{si} + (\rho_{air} + \rho_{si})\phi \qquad (8)$$

$$\mu = \mu_{si} + (\mu_{air} + \mu_{si})\phi \qquad (9)$$

$$k = k_{si} + (k_{air} + k_{si})\phi \tag{10}$$

$$C_p = C_{psi,eff} + (C_{pair} + C_{psi,eff})\phi \tag{11}$$

In this model, when the monocrystalline silicon target is vaporized under the action of a high-energy density laser, two source terms are added to Equation 1 and 7 after being multiplied for the function δ. This prevents the vaporization process from only occurring within the thin layer area of the interface and the process is in agreement with the mass transfer process. This function can be expressed as:

$$\delta = 6|\phi(1-\phi)|\|\nabla\phi\| \tag{12}$$

when the vaporization occurs, the vapor velocity $\vec{u}_v$, the interface velocity $\vec{u}_{int}$, and the liquid velocity $\vec{u}_L$ are different and depend on the vapor phase transition gas dynamics. Their relation can be expressed as follows:

$$\vec{u}_{int} \cdot \vec{n} = \vec{u}_L \cdot \vec{n} - \frac{\dot{m}}{\rho_L} \tag{13}$$

$$\vec{u}_{int} \cdot \vec{n} = \vec{u}_v \cdot \vec{n} - \frac{\dot{m}}{\rho_v} \tag{14}$$

By substituting Equation 13 into Equation 14, the natural boundary condition of the interface becomes:

$$\vec{n} \cdot \vec{u}_v - \vec{n} \cdot \vec{u}_L = \dot{m}(\frac{1}{\rho_v} - \frac{1}{\rho_L}) \tag{15}$$

Here, $\dot{m}$ corresponds to the evaporative mobility, and outside the interfaces are all incompressible Newtonian laminar flow. In order to define the interface with a value and to define the rest of sample as zero, the continuous source term is modified by multiplying it for the function δ. The mass conservation equation is modified and the source term is added to it. By substituting it into Equation

(15) the following equation can be obtained:

$$\nabla \cdot \vec{u} = \delta\dot{m}(\frac{1}{\rho_v} - \frac{1}{\rho_L}) \cdot \vec{n} \tag{16}$$

Since only the interface convection is usually taken into consideration and the movement of the interface caused by evaporation is often neglected, the level set control equations can be modified as follows:

$$\frac{\partial\varphi}{\partial t} + \vec{u} \cdot \nabla\varphi - \delta\dot{m}(\frac{V_{f,v}}{\rho_v} + \frac{V_{f,L}}{\rho_L}) +$$
$$+ \gamma[(\nabla \cdot (\varphi(1-\varphi)\frac{\nabla\varphi}{|\nabla\varphi|})) - \varepsilon\nabla \cdot \nabla\varphi] = 0 \tag{17}$$

Here, the initial temperature is $T_0 = 300 K$.

At the interface between the gas and the liquid phases, the hydrodynamic boundary condition is the following:

$$[-pI + \mu(\nabla\vec{u}) + (\nabla\vec{u})^T]\vec{n} = \vec{F} \tag{18}$$

The other boundaries can be described by the following adiabatic boundary condition:

$$-k\nabla T = 0 \tag{19}$$

2.3. Numerical results and analysis

Fig. 2 shows the two-dimensional cross section view of the simulation of monocrystalline silicon instantaneous morphology under a single laser pulse. When the monocrystalline silicon is damaged by the millisecond pulse laser and ablation occurs, the thermal diffusion and the subsequent boiling process cause an increase in the etch pit depth.
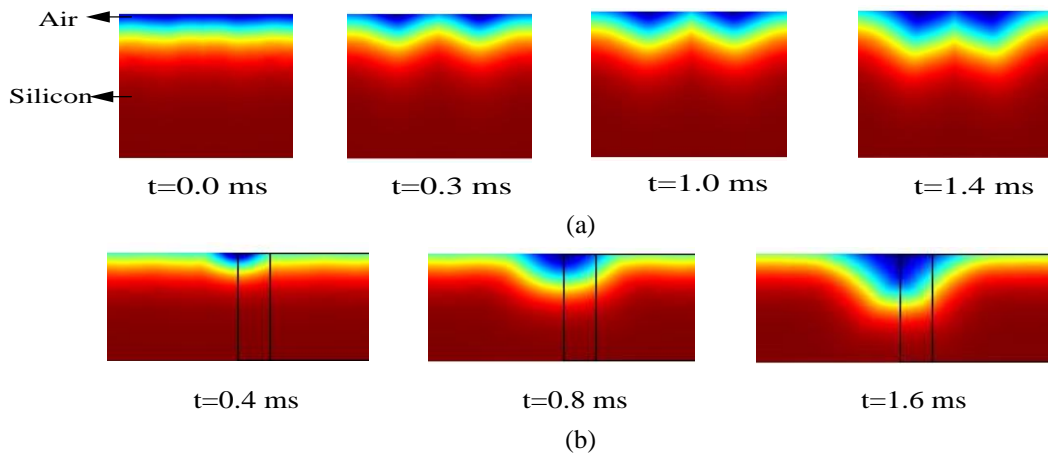
Fig. 2. Two-dimensional cross-section of the monocrystalline silicon instantaneously upon melting ((a)τ_p=1.0 ms, Ep=191.1 J/cm^2;(b) τ_p=1.0 ms, Ep=317.8 J/cm^2) (color online)

Fig. 2(a) shows: (1) The high-energy density laser instantaneously generates a high temperature when it acts on the monocrystalline silicon targets. Evaporation and spatter take place within the laser radiation area not only during the laser irradiation time but also after the laser stops irradiating. The depth increases by a certain amount after the irradiation stops. This mainly happens because the laser energy is absorbed by the target and it increases upon an increase in the laser energy density. The higher the laser energy density is, the longer it takes to spread the heat. (2) Since the laser energy mainly concentrates at the bottom of the ablation pit, a large back pressure is generated at the bottom of the pit. The gas dynamics results in a strong backflow. The back pressure causes the fluid to flow upwards and the ablation pit forms. At the beginning of the ablation pit formation process, the molten fluid can be easily pushed upwards out of the pit due to the back pressure. As the depth of the pit increases, the molten fluid cannot be effectively pushed out of the pit, especially if it is located at its bottom, and even when a high back pressure is exerted on the pit. Since the viscous shear stress weakens the upward momentum of the fluid, and

both the hydrodynamic pressure and the surface tension induce the downward flow of the ablation pit fluid, the reverse flow and the collision form a bulge: the pit with a "spike" structure appears.

Fig. 2(b) shows that with the increase of the laser energy density, the shape of the molten pool generated by the high-energy density laser irradiation exhibits a crater structure: The temperature of the center, where the laser irradiation takes place, is high and the temperature gradient is large. The temperature gradient induces a thermal capillary flow that forms a crater structure. During the formation and the stabilization of the ablation pits, the Magnunes effect only has a very weak effect when compared to recoil pressure and surface tension.

Fig. 3 shows the relation between the ablation depth changes and the changes in energy density and in pulse width under the following conditions: the laser output mode is single pulse, the spot radius is 1.0 mm, the pulse width measures 1.0 ms, and the laser energy density is 165.6 J/cm^2.

(a)

(b)
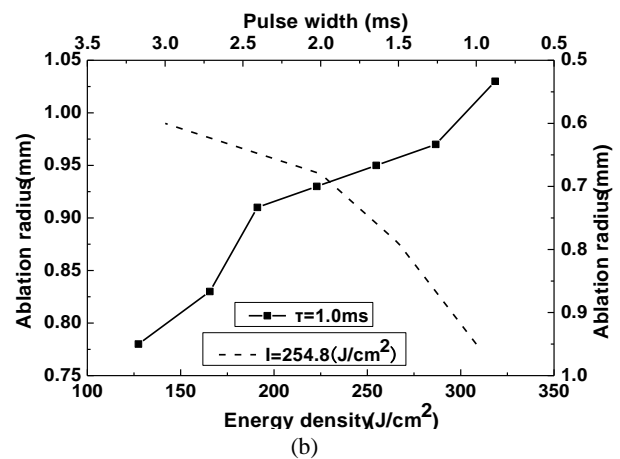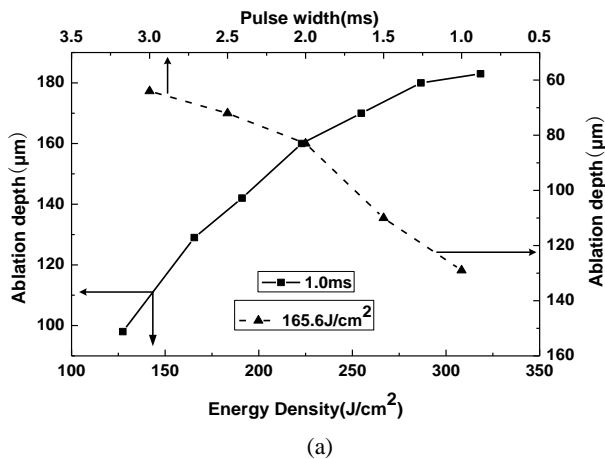
Fig. 3. Variation of the ablation depth as a function of energy density and pulse width

Fig. 3(a) shows that for a fixed laser pulse width, the ablation depth of the monocrystalline silicon damaged by the millisecond pulse laser increases upon the increase in the laser energy density. With the increase of the laser energy density, the monocrystalline silicon target absorbs a higher laser energy. For this reason, the melting and vaporization velocity increase, as well as ablation depth. For a fixed laser energy density, the laser power density becomes smaller, the melting and vaporization time increase, and the etch depth decreases upon the increase in the pulse width. It can be seen from Fig. 3 (b) that for a fixed laser pulse width, the erosion radius of monocrystalline silicon increases with the increase in laser energy density. With a constant laser energy density, the ablation radius decreases upon an increase in the pulse width.

3. Experiment

3.1. Experimental facility

The experimental system, which includes a millisecond pulse laser and a single crystal silicon sample is shown in Fig. 4. The laser used in this experiment is a Melar-100Nd:YAG pulsed laser with a repetition rate of 10 Hz, a wavelength of 1064 nm, a pulse width of 1.0–3.0 ms, an adjustment step of 0.5 ms, a Gaussian laser intensity spatial distribution, a pulse repetition frequency of 10 Hz. Moreover, the laser is used in a single pulse or pulse train mode. After the output beam passes through a beam splitter, one part travels through a dichroic prism and enters the VEGA FL500A's energy meter to measure the laser energy. The other part travels through a single lens via a focusing lens. The diameter of the spot on the surface

of the crystalline silicon sample after focusing measures approximately 2.0 mm. A series of monocrystalline silicon

samples were clamped on a five-dimensional translation stage.
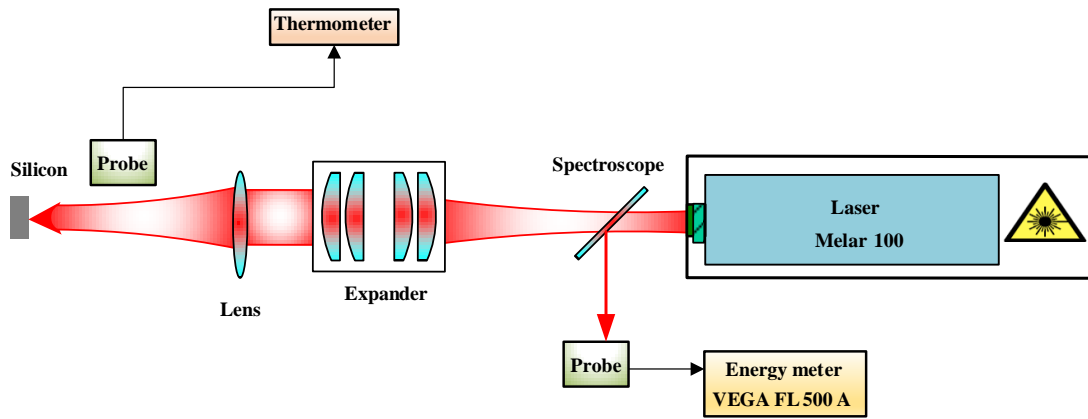
Fig. 4. Experimental system to ablate the monocrystalline silicon sample (color online)

3.2. Experiment results and analysis

3.2.1. Analysis of erosion depth

The three-dimensional surface measuring instrument with an automatic zoom function was used to measure three-dimensional morphology of monocrystalline silicon targets, and the ablation depth data was obtained after being processed with particular software.
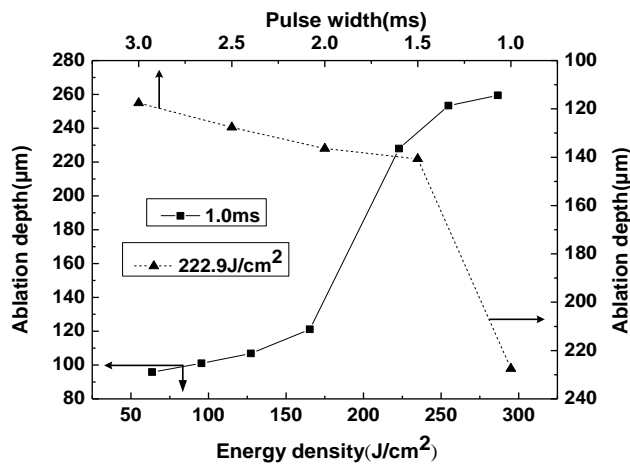
Fig. 5. Relation between ablation depth and energy density and the pulse width

Fig. 5 shows the relation between the variation in ablation depth of monocrystalline silicon and both the laser energy density and the pulse width when the laser is operated in single pulse. The laser ablation depth increases with the increase of the laser energy density for a fixed pulse width. Furthermore, the laser ablation depth decreases upon the increase in the pulse width for a fixed pulse laser energy density. When the laser energy density remains constant and the pulse width increases, the laser power density becomes smaller and the temperature of the irradiated center point decreases. The temperature of the

central point of the target surface can be determined by the laser power density. Increasing the laser pulse width is equivalent to increasing the duration of the irradiation when the laser energy remains unchanged and the heat conduction time increases. A higher amount of energy is lost during the heat conduction process, and the temperature rise rate is slower to achieve melting and gasification. As the time becomes longer, the speed of the mass migration caused by splashing and gasification becomes slower, as well. As a result, the ablation depth and the radius of the melt hole decrease as the pulse width increases.
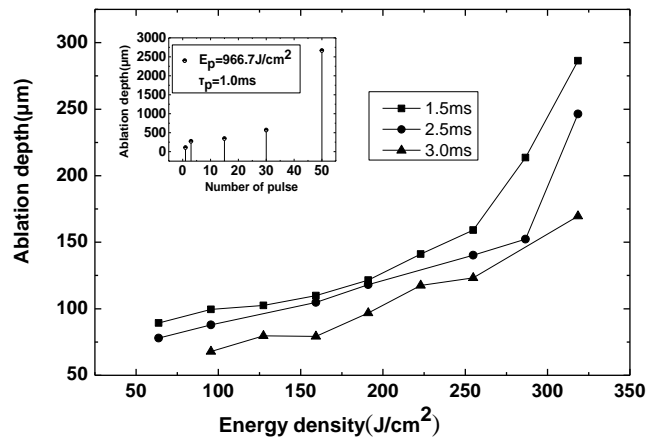
Fig. 6. Ablation depth as a function of the laser energy density and the number of pulses

Fig. 6 shows the variation in the ablation depth of monocrystalline silicon as a function of the laser energy density and the pulse width in single pulse. For a fixed pulse laser energy density, the laser ablation depth decreases with the increase in the pulse width. When the laser energy density is lower than 200.0 J/cm^2, the ablation depth of monocrystalline silicon does not change significantly. When the laser energy density is higher than 200.0 J/cm^2, the monocrystalline silicon ablation depth

increases rapidly upon an increase in laser energy density.

Fig. 6 shows the relation between the ablation depth and the number of pulses: The ablation depth increases with the increase in the number of pulses. When the number of pulses is larger than 30, the ablation depth increases sharply.

3.2.2. Comparison of the experimental and simulation results

Fig. 7(a) shows the comparison between the simulated morphology of laser-damaged monocrystalline silicon and the experimental measurements with a pulse width of 1.0 ms and a pulse energy density of 191.1 J/cm^2. It can be seen from Fig. 10 that the experiment is in good agreement with the theoretical results and it verifies the physical model behind the laser damaged monocrystalline silicon ablation process. Fig. 7(b) shows the comparison between the experimental and the simulated results of the ablation depth on the monocrystalline silicon target generated by a millisecond pulsed laser. Fig. 7(b) shows that when the laser energy density is in the 63.7–191.1 J/cm^2 range, the monocrystalline silicon ablation depth is in the 95.8–168.2 μm range, whereas the simulated monocrystalline silicon ablation depth is in the 77.4–142.5 μm range. The experimental and numerical simulation results are almost identical, and the ablation depth increases with the increase of the laser energy density.

(a)

(b)
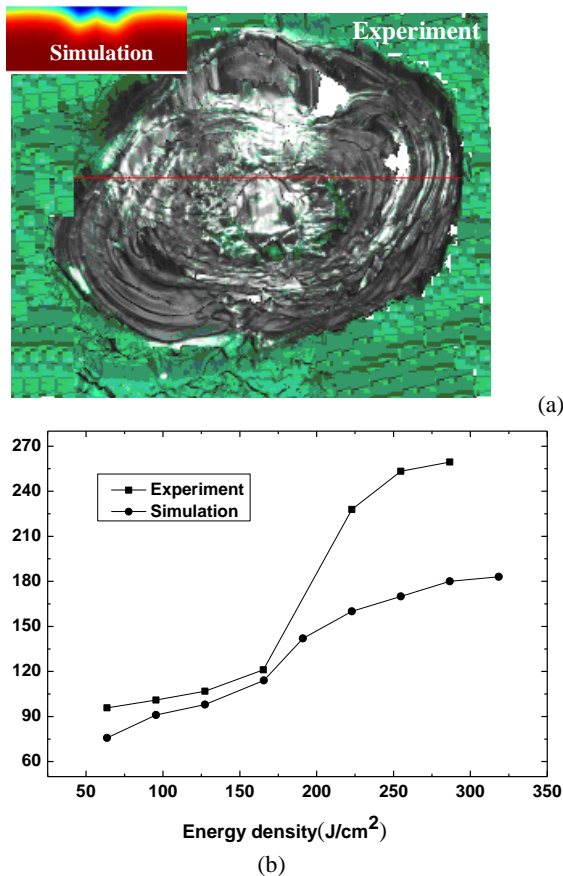
Fig. 7. Comparison between experimental and simulated results. ((a) τ$_p$=1.0 ms, E$_p$ =191.1J/cm^2; (b) τ$_p$=1.0 ms) (color online)
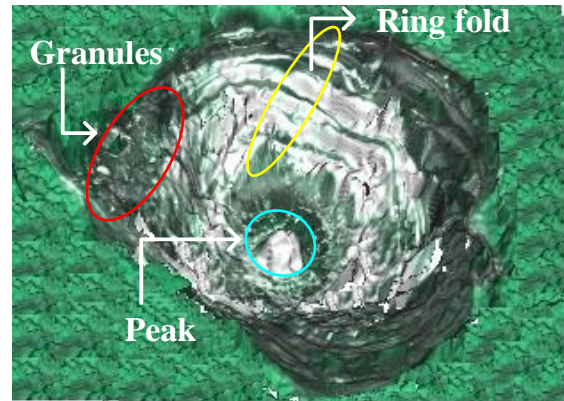
Fig. 8. Damage morphology of the monocrystalline silicon sample (color online)

Fig. 8 shows the morphology of a monocrystalline silicon target irradiated by a millisecond laser with an energy density of 318.5 J/cm^2. The image was acquired via the IFM G4 auto-zoom three-dimensional surface measuring instrument. It can be seen from the figure that a high-energy millisecond pulse laser irradiates monocrystalline silicon, there are obvious ablation pits in the laser damaged area. The size and the depth of the pits are closely related to the laser light field distribution and to the unevenness of the target material. A protruding peak structure appears in the center of the molten pool, and the surface of material generates a tension. When this tension is small, it can be elastically absorbed by monocrystalline silicon. A larger tension induces the molten silicon to flow toward the center, forming a peak shape in the center of the molten pool structure: in this case, the stress damage area and the splash area are mixed together, and the damage area gradually increases. Particulate matter appears on the surface of the monocrystalline silicon sample, and droplet ejection occurs. This phenomenon takes place due to the phase explosion and the explosive boiling, which is consistent with the ejection mechanism of the droplets described by the ablation theory. During the damage process, a large amount of plasma carrying thermal energy is generated. The bulk expansion generates a large impact pressure on the monocrystalline silicon. Consequently, the liquid material generated during the action of the laser is sputtered out and particle spattering it is visible.

4. Conclusion

In this paper, the simulation and the experimental results on the millisecond pulse laser effect on a monocrystalline silicon sample are presented. In the simulation, the improved level set method is used to track the vapor-liquid interface. The simulation and erosion morphology detected experimentally are consistent. When the monocrystalline silicon is damaged by the millisecond pulsed laser, no obvious ablation pit is visible: The thermal diffusion and the subsequent boiling are the main reasons

for the increase in the pit depth, which is also related to the laser light field distribution and the target uniformity. The appearance of a "spike" in the pit is mainly induces by the collision between the upward and the downward flow, which results from the backward and the surface tensions. For a fixed laser pulse width, the ablation depth of the sample increases with the increase in the laser energy density. For a fixed laser energy density, as the pulse width increases, the laser power density becomes smaller, the melting and vaporization times become longer, and the blation depth and ablation radius decrease. When the laser stops irradiating, the heat generated by the laser energy absorbed by the target is not fully transported through the sample. A longer time is necessary for this process to take place and the ablation depth continues to increase after irradiation. The ablation depth increases rapidly with the increase in the number of pulses. The results of this study provide a theoretical and experimental reference on the investigation of the resisting laser damage on monocrystalline silicon.

Acknowledgment

References

[1] Andrea Lübcke, Zsuzsanna Pápa, Matthias Schnürer, Applied Sciences **9**(17), 3636 (2019).

[2] S. He, J. J. Nivas, A. Vecchione et al., Optics Express **24**(4), 3238 (2016).

[3] S. Huang, X. D. Ruan, F. U. Xin et al., Journal of Zhejiang University-Science A (Applied Physics & Engineering) **10**(1), 7 (2009).

[4] R. N. Raman, R. A. Negres, P. Demange et al., Proceedings of SPIE - The International Society for Optical Engineering 7581:75810D-75810D-11 (2010).

[5] J. Liu, X. Jia, W. Wu et al., Optics Express **26**(5), 6302 (2018).

[6] Y. Pan, X. Lv, H. Zhang et al., Optics Letters **41**(12), 2807 (2016).

[7] Jörn Bonse et al., IEEE Journal of Selected Topics in Quantum Electronics 23.3 (2016).

[8] Zhi-Chao Jia, Ze-Wen Li, Jie Zhou et al., Chin. Phys. B **26**(11), 116102 (2017).

[9] Q. Zheng, Z. Fan, G. Jiang et al., Optics Express **27**(19), 16 (2019).

[10] G. D. Gautam, A. K. Pandey, Optics & Laser Technology **100**, 183 (2018).

[11] Bo-Shi Yuan, Wang et al., Applied Optics **57**(20), 5743 (2018).

[12] S. Tao, B. Wu, Y. Zhou et al., Journal of Applied Physics **106**(12), 457 (2009).

[13] C. Fornaroli, J. Holtkamp, A. Gillner, Physics Procedia **41**, 603 (2013).

[14] O. Armbruster, A. Naghilou, M. Kitzler et al., Applied Surface Science **396**, 1736 (2017).

[15] R. K. Endo, Y. Fujihara, M. Susa, High Temp High Press **35**(36), 505 (2003).

[16] K. Yamaguchi, K. Itagaki, Journal of Thermal Analysis & Calorimetry **69**(3), 1059 (2002).

[17] I. D. Vrinceanu, S. Danyluk, Measurement of residual stress in single crystal silicon wafers[C]// International Symposium on Advanced Packaging Materials, 2002 Proceedings IEEE, 297 (2002). (https: //ieeexplore. ieee. org/document/990402/).

[18] R. F. Wood, Pulsed laser processing of Semiconductors, Semiconductors and Semimetals 23, Cha 6, 1984.

_____
*Corresponding author: laserqit@sina.com